Magnetic Moment Collapse-Driven Mott Transition in MnO

Jan Kuneš[1,2,*] Alexey V. Lukoyanov[3], Vladimir I. Anisimov[4],
Richard T. Scalettar[5], and Warren E. Pickett[5]

[1] *Theoretical Physics III, Center for Electronic Correlations and Magnetism, Institute of Physics, University of Augsburg, Augsburg 86135, Germany*

[2] *Institute of Physics, Academy of Sciences of the Czech Republic, Cukrovarnická 10, 162 53 Praha 6, Czech Republic*

[3] *Ural State Technical University-UPI, 620002 Yekaterinburg, Russia*

[4] *Institute of Metal Physics, Russian Academy of Sciences-Ural Division, 620041 Yekaterinburg GSP-170, Russia and*

[5] *Department of Physics, University of California Davis, Davis, California 95616*

(Dated: December 19, 2008)

The metal-insulator transition in correlated electron systems, where electron states transform from itinerant to localized, has been one of the central themes of condensed matter physics for more than half a century. The persistence of this question has been a consequence both of the intricacy of the fundamental issues and the growing recognition of the complexities that arise in real materials, even when strong repulsive interactions play the primary role. The initial concept of Mott was based on the relative importance of kinetic hopping (measured by the bandwidth) and on-site repulsion of electrons. Real materials, however, have many additional degrees of freedom that, as is recently attracting note, give rise to a rich variety of scenarios for a "Mott transition." Here we report results for the classic correlated insulator MnO which reproduce a simultaneous moment collapse, volume collapse, and metallization transition near the observed pressure, and identify the mechanism as collapse of the magnetic moment due to increase of crystal field splitting, rather than to variation in the bandwidth.

We consider, as one of the simpler examples of the canonical Mott insulators,[1,2] the rocksalt structure transition metal monoxide (TMMO) manganese oxide with half-filled $3d$ shell. MnO is, most certainly, a multiorbital multielectron system with the accompanying complexities of the tenfold degeneracy, but the half-filled $3d$ states under ambient conditions lead to a spherical spin-only magnetic moment. Applying pressure to such a system leads to a number of changes, including insulator-metal transition, orbital repopulation, moment reduction, and volume collapse if a first-order transition results. These changes may occur simultaneously, or sequentially over a range of volumes.[3] Any of these may be accompanied by a structural phase transition, that is, a change in crystal symmetry, but an isostructural volume collapse may occur as well. The $3d$ bandwidth of such a Mott insulator is very susceptible to applied pressure, and has been thought to be one of the main controlling factors in the transition.

While MnO's half-filled shell seems to give it a connection to well studied models, this aspect also makes it atypical of transition metal monoxides, as shown by Saitoh *et al.* who compiled[4] effective parameters for TMMOs from spectroscopic information. An effective intra-atomic Coulomb repulsion energy U_{eff} as defined by them is roughly twice as large as for the other $3d$ monoxides, and this has been used to suggest that MnO may be the most strongly correlated TMMO. The complexity that should be expected can be grasped by listing the relevant energy scales: $3d$ band-

width W, Coulomb repulsion U, intra-atomic $d-d$ exchange energy (Hund's rule) J, crystal field splitting $\Delta_{cf} = \varepsilon_{e_g} - \varepsilon_{t_{2g}}$, and charge transfer energy $\Delta_{ct} \equiv \varepsilon_{t_{2g}} - \varepsilon_p$ [the difference in Mn $3d$ (we use t_{2g}) and O $2p$ site energies]. All of these scales evolve as the volume decreases, altering the various microscopic processes and making the pressure-driven Mott transition a challenging phenomenon to describe.

Early shock data[5], and then Raman and optical studies,[6,7] had identified a transformation in MnO in the neighborhood of 90-105 GPa. Transport,[8] magnetic,[8] structural and spectroscopic,[9,10] and reflectivity[6] data all point to a first-order, insulator-metal Mott transition near 100 GPa with (reduced) volume ($v = V/V_\circ$) collapse v=0.68→0.63, and moment collapse (from $\sim 5\mu_B$ to $1\mu_B$ or less[9,10]). The structural data indicates a B1→B8 change just before the Mott transition, which thus occurs within the B8 (NiAs) phase rather than the B1 (NaCl) phase. Since the local environment of the Mn ion remains the same, this structural change is not expected to have much effect on the Mott transition in the disordered phase.

Dynamical mean field theory (DMFT)[11–13] as an approach for studying real materials has been showing impressive successes.[14? –21] The method that we have implemented and applied (see Methods section below) moves the treatment significantly beyond the methods used earlier for TMMOs, by including a full thermodynamic average of local dynamic processes resulting from the strong interaction and all orbitals that can be relevant. Cohen, Mazin, and Isaak calculated the energy and magnetic moment using only local density approximation (LDA) based interactions.[23] In LDA MnO metalizes at (much too) low pressure; within the metallic phase they obtained a moment and volume collapse around 150 GPa. Fang and collaborators addressed this difficulty by using LDA only for the high pressure phase, and modeling the low pressure phase with the correlated LDA+U method.[24] With two different functionals, however, it is not possible to obtain the transition pressure. Four correlated electronic structure methods[25], applied throughout the volume range of interest, have probed the behavior of MnO under pressure; all obtained a high spin (HS, $S = \frac{5}{2}$) to low spin (LS, $S = \frac{1}{2}$) moment collapse but their predictions differed considerably in other respects, demonstrating that the specific treatment of correlation effects is crucial. The prediction of the LDA+U method, which is regarded as the static, T=0 limit of the LDA+DMFT theory used here, is found to be affected by magnetic order,[26] and predicts a zero temperature moment collapse in an insulator-insulator transition around 120 GPa (the pressure depends on the value of J), with little difference between the B1 and B8 structure results. Thermodynamic fluctuations have not been included in any previous study of MnO.

Magnetic Moment Collapse and Metallization

Following most closely the approach developed and implemented by McMahan, Held, and Scalettar[27–29] for pressure studies of elemental lanthanides, we have addressed the pressure-driven collapse of the correlated insulating state, using MnO as the prototype. Fig. 1 illustrates the evolution of the local magnetic moment and Mn $3d$ occupancies with volume. We use two different measures of the local moment: (a) the mean instantaneous moment defined as an equal time correlation function $M_s = \sqrt{\langle \hat{m}_z^2 \rangle}$ and (b) effective local moment defined through the local spin susceptibility $M_{eff} = \sqrt{T\chi_{loc}}$. These two moments have similar T-independent values in materials with Curie-Weiss behavior. Under compression, the local moment and Mn $3d$ orbital occupancies retain their ambient pressure HS values ($S = \frac{5}{2}$) down to about v=0.68. Further compression rapidly degrades the moment, which is accompanied by redistribution of electrons $e_g \rightarrow t_{2g}$ within the Mn $3d$ shell. The local moments and orbital occupancies start to level off to the LS values around $v = 0.57$. The reduction of M_{eff} below M_s in the LS state indicates that the local moment screening (charge fluctuations) is enhanced in comparison to the HS state.

Next we address the spectral properties, where the shortcomings of the LDA spectrum have been clear for decades. In Fig. 2 we compare the calculated total Mn $3d$ spectral function at ambient pressure with the photoemission data of van Elp *et al.*[30]. Excellent agreement is obtained for the gap and for the peak positions. (We note that using the enhanced value of J=1 eV gives significantly poorer agreement.) Having obtained a correct ambient pressure spectrum, we proceed in the study of the Mott transition by following the evolution with decreasing volume of the symmetry-resolved (t_{2g}, e_g) spectral densities, presented in Fig. 3. The onset of the moment collapse around $v = 0.68$ is signaled by, and associated with, closing of the gap in the t_{2g} channel, while the e_g gap is still visible at $v = 0.63$. This orbital selectivity[31,32] in metalization cannot be an exact property since both e_g and t_{2g} bands hybridize with the same O $2p$ bands throughout the Brillouin zone; however, the smallness of t_{2g}–$2p$ mixing allows the orbital selectivity to be remarkably pronounced. As the t_{2g} gap closes, a quasiparticle peak appears at the chemical potential (E=0) as has been seen in simple models.[12] Once in the LS state, the spectral functions bear strong resemblance to the parent LDA bands. In particular, the LDA ($U = J = 0$) t_{2g} spectrum contains a sharp peak just at/below the chemical potential, so it is not certain how much of the peak arising at the transition is due to the many-body nature of the system.

Mechanism of the Mott Transition in MnO

We now address a fundamental point of this work, namely the connection between moment collapse and metal-insulator transition, by observation of the impact of pressure on the effective Hamiltonian. Since U and J do not change, the pressure enters the calculation only through the quadratic (one-electron) part of the effective Hamiltonian. Reducing the role of pressure down to fundamentals one ends up with two effects: (i) broadening of the $3d$ bands and (ii) increase of the crystal-field splitting Δ_{cf}. (We define Δ_{cf} in terms of the site energies of the e_g and t_{2g} Wannier functions; the e_g–t_{2g} band splitting is substantially larger due to ligand field effects.) The evolution of the leading band structure quantities, which are the nearest-neighbor hopping amplitude $t_{pd\sigma}$, Δ_{cf}, and Δ_{ct}, are shown in the inset of Fig. 5. Since the $3d$ bandwidth arises mainly through Mn $3d$ – O $2p$ hybridization ($W \propto t_{pd}^2/\Delta_{ct}$) the increase of t_{pd} hopping with pressure is to some extent compensated by the overall lowering of the p bands (increase in Δ_{ct}).

So far we have demonstrated a connection between the moment collapse and metal-insulator transition (MIT), yet the chicken-and-egg question – which property drives? which property follows? – is not yet answered. To this end we have performed an additional calculation at $v = 0.8$ (well within the insulating HS state) without *any* intra-atomic exchange (J=0). In spite of the large U and same U/W ratio, a LS solution is obtained, which is metallic although strongly renormalized. This result clearly shows that the MIT is *driven by the collapse of the moment*, which cannot withstand the increase of Δ_{cf}. The transition is characterized as evolving from five half-filled bands $t_{2g} + e_g$ (HS) to three t_{2g} bands with one hole per site (LS). The interaction energy cost of moving an electron from site to site is determined by $U_{eff} = d^{n+1} + d^{n-1} - 2d^n$. Using the atomic configurations corresponding to HS and LS states one arrives at an *effective* repulsion[33] $U_{eff}^{HS} = U + 4J = 10.3$ eV and $U_{eff}^{LS} = U - J = 5.9$ eV respectively, indicating much stronger inhibition of the electron propagation in HS state. Moreover, the Mn $3d(e_g)$ – O $2p$ hybridization provides an additional screening channel for the effective $t_{2g} - t_{2g}$ interaction in the LS state. Indeed, a calculation performed in the LS state with O $2p$ states integrated out (keeping the $3d$ bandwidth unchanged) before solving the interacting problem leads to more pronounced high energy shoulders as compared to the solution with O-p states fully included; an indication of stronger local correlations.

These results establish that the transition is controlled by competition between the crystal-field

spitting Δ_{cf} (favoring the LS state) and the intra-atomic exchange coupling J (favoring the HS state). Although both energy scales are important for the outcome of the calculations, only the former (Δ_{cf}) is sensitive to an applied pressure. The importance of the value of J was also found in LDA+U studies of the Mott transition.[26] Recently Werner and Millis[34] studied a two band model with competing intra-atomic exchange and crystal-field splitting. In the parameter range relevant for the present study they found three different phases realized in the following order with increasing crystal-field splitting: (i) spin-polarized Mott insulator, (ii) metal with large orbital and spin fluctuations and (iii) orbitally polarized insulator. Moreover they found an orbitally selective closing of the gap upon doping in the vicinity to the (i)-(ii) phase boundary. The correspondence between their spin-polarized insulator phase (i) and the HS state of MnO is evident. The transition region in MnO and phase (ii) are both characterized by metallization and strong orbital fluctuations as well as the orbitally selective gap behavior. Also the LS state of MnO and the phase (iii) of the model exhibit similarity, the orbital polarization. The insulating character of their phase (iii) is dictated by band-filling and does not contradict the above analogy.

Like almost all previous studies using LDA+DMFT, we have included only the density-density terms of the Coulomb repulsion. Although they are not expected to influence a first-order volume collapse (see the next section) especially above 1000 K, it is gratifying to obtain some confirmation. Werner and Millis used the full Coulomb interaction in their study, and the similarity of the behavior of their model to what is found here for MnO provides some verification of the unimportance of the neglected terms.

Equation of State and the Critical Pressure

To compare to high pressure experiments, knowledge of phase stability is needed, which can be obtained from free energy vs volume (equation of state EOS). The theoretical justification for applying DMFT using the underlying LDA description relies on a well-defined thermodynamic grand canonical potential functional, for which specific realizations have been suggested.[15,27,35] Since it is difficult to extract the entropic term[28] in the free energy we restrict ourselves to evaluation of the internal energy; in any case the variation of the entropy term is very small on the energy scale of several eV involved in the changes of total energy. We use the internal energy scheme of McMahan *et al.*[15,27–29] that is similar to that of Savrasov and Kotliar[35] corresponding to the expression $E(V,T) = E_{LDA}(V) + [E_{DMFT}(V,T) - E_{MF}(V)]$, where E_{LDA} is the all-electron (unpolarized) LDA energy, E_{DMFT} is the internal energy corresponding to the self-consistent (dynamic) DMFT solution for the effective Hamiltonian and E_{MF} is the static mean-field internal energy. The EOS curve is shown in Fig. 5. The main feature is the deviation from convexity in the transition region, which leads to a calculated volume collapse $v^{th} = 0.68 \rightarrow 0.59$ at $P_c^{th} = 120$ GPa. The metallization and moment collapse obtained here are not far from the high pressure data,[8–10] with the transition volume (pressure) being somewhat smaller (larger) than the experimental values $v_c^{exp} = 0.68 \rightarrow 0.63$, $P_c^{exp} = 100$ GPa. The state just above the collapse is a HS insulator, with the t_{2g} gap about to close. The collapsed state is LS, the e_g gap having just closed making it metallic in both subshells.

Summary and Outlook

These results demonstrate that the underlying LDA band structure, buttressed by on-site interactions (U, J) treated within the dynamical DMFT ansatz, provide a realistic description of the Mott transition in MnO without input from experiment. This study finally allows a determination of the mechanism of the transition, which could not be uncovered by experiment alone: the magnetic moment collapse, volume collapse, and metal-insulator transitions occur simultaneously, but it is the increasing crystal field splitting (encroachment of the O^{2-} ion on the internal structure of the Mn ion) and not the increasing bandwidth that tips the balance.

The current results illustrate success of the LDA+DMFT approach in describing a pressure-

driven Mott transition in a strongly correlated insulator, joining the growing number of successes of this approach in other strongly correlated real materials. The Kondo volume collapse transition in Ce[15,28] and other elemental lanthanides,[29] and the realistic modeling of parts of the complex phase diagram[16] and multiplet effects[36] in Pu reflect the progress in correlated metals, with low temperature properties (heavy fermion characteristics) remaining an imposing challenge. Impressive progress has also been demonstrated in the description of structurally-driven[17,37] and doping-driven[38] metal-insulator transitions in transition metal oxides. Excitation spectra[21,22] of the charge-transfer compound NiO at ambient pressure, where O $2p$ states are tangled with the $3d$ states, have shown excellent agreement with experiment. These results on MnO bring an additional class of materials into the list of strongly correlated systems whose behavior is becoming understood due to recent theoretical developments.

Theoretical Approach and Numerical Methods

Single Particle Hamiltonian and Interaction Term

The LDA+DMFT computational scheme[19] in its present implementation, applied previously to NiO,[21,22] proceeds in two steps: (i) construction of an effective multi-band Hubbard Hamiltonian H via Wannier transformation from a converged (unpolarized, metallic) LDA solution corrected for double-counting of the on-site interaction, and (ii) self-consistent solution of the DMFT equations[12,20] using the quantum Monte-Carlo impurity solver.[39]

$$\begin{aligned} H \;=\; & \sum_{\mathbf{k},\sigma,\alpha,\beta} h^{dd}_{\mathbf{k},\alpha\beta} d^{\dagger}_{\mathbf{k}\alpha\sigma} d_{\mathbf{k}\beta\sigma} + \sum_{\mathbf{k},\sigma,\gamma,\delta} h^{pp}_{\mathbf{k},\gamma\delta} p^{\dagger}_{\mathbf{k}\gamma\sigma} p_{\mathbf{k}\delta\sigma} + \sum_{\mathbf{k},\sigma,\alpha,\gamma} h^{dp}_{\mathbf{k},\alpha\gamma} d^{\dagger}_{\mathbf{k}\alpha\sigma} p_{\mathbf{k}\gamma\sigma} + \sum_{\mathbf{k},\sigma,\gamma,\alpha} h^{pd}_{\mathbf{k},\gamma\alpha} p^{\dagger}_{\mathbf{k}\gamma\sigma} d_{\mathbf{k}\alpha\sigma} \\ & + \sum_{i,\sigma,\sigma',\alpha,\beta} \mathcal{U}^{\sigma\sigma'}_{\alpha\beta} n^{d}_{i\alpha\sigma} n^{d}_{i\beta\sigma'}, \end{aligned}$$

where $d_{\mathbf{k}\alpha\sigma}$ ($p_{\mathbf{k}\gamma\sigma}$) is the Fourier transform of the operator $d_{i\alpha\sigma}$ ($p_{i\gamma\sigma}$), which annihilates the d (p) electron with orbital and spin indices $\alpha\sigma$ ($\gamma\sigma$) in the ith unit cell, and $n^{d}_{i\alpha\sigma}$ is the corresponding d occupation number operator.

The single particle part of the Hamiltonian was obtained by a Wannier function projection method[40], which amounts to a unitary transformation in the Hilbert space containing Mn $3d$, O $2p$ bands and the next lowest empty (polarization) conduction band. The site energy of the Mn $3d$ orbitals was corrected for double counting of the $d-d$ interaction by subtracting from the LDA site

energy ε_d a Hartree-like term giving $\varepsilon_d^\circ = \varepsilon_d - (N-1)\bar{U}n_{LDA}$, where $N = 10$ is the total number of orbitals per Mn site, $\bar{U}$ is the average Coulomb repulsion and n_{LDA} is the average occupancy per d-orbital. Since the $p-d$ band separation Δ_{ct} in MnO, which is to some extent influenced by the choice of the double-counting term, is rather large in the transition region, small variation of Δ_{ct} will not change the results.

The Coulomb Interaction Matrix

The on-site Coulomb interaction $\mathcal{U}_{\alpha\beta}^{\sigma\sigma'}(U,J)$ within the Mn $3d$ shell, restricted to density-density terms only, was expressed as usual[41] in terms of the direct (U) and exchange (J) interaction strengths related to the Slater integrals F_0, F_2, F_4. The numerical values[33] of U=6.9 eV and J=0.86 eV were obtained by the constrained LDA method[42]. Since they exhibit only a small pressure dependence, these values were used for all volumes. We used L=100 imaginary time points in the Monte-Carlo simulation, in which the standard single-field-flip moves were augmented by special global moves that played a crucial role in ensuring ergodic sampling in the transition region. To obtain an indication of the robustness of our results we perform, in parallel with these *ab initio* interaction strengths, calculations with an enhanced (by 15%) value of J=1 eV (and fixed U/J ratio). All the presented results were obtained at the temperature T=1160 K, in the rocksalt structure.

Monte Carlo Procedure; Introduction of Global Moves

The DMFT equations were solved numerically on a Matsubara contour (using asymptotic expansions for frequencies $\omega_n > 500$ eV), and the k-space integrals were performed by summation over 3375 k-points in the first Brillouin zone. The chemical potential was adjusted in each DMFT iteration to guarantee the total electron count of 11 ± 10^{-6}. The impurity problem was solved using the Hirsch-Fye QMC algorithm[39] modified for multiple orbitals. The on-site interaction was decoupled using a single binary Hubbard-Stratonovich auxiliary field $S_{\alpha\beta}(l)$ for each pair of orbitals $\alpha\beta$ and each of L imaginary time slices (45 auxiliary fields for each time slice).

The key innovation in this application to MnO in the transition regime was introduction of global Monte-Carlo moves in addition to the usual single-flips of the auxiliary fields. These moves allow for fluctuations between HS- and LS-like configurations, which are otherwise practically unreachable with the standard single-auxiliary-field-flip moves. The purpose of global moves is to mimic transferring electrons between orbitals. In general there is no straightforward relationship between a given configuration of auxiliary fields, described by a binary L-vector $S_{\alpha\beta}$ and the occupancy of

orbitals. However, in the case of two atomic orbitals the probability distribution is peaked around auxiliary field configurations corresponding to a particular orbital occupancy, and flipping all fields corresponds to swapping occupancies of the two orbitals[43]. This can be generalized to multiple orbitals as follows. To swap occupancies of orbitals α and β one has to: (1) flip fields in $S_{\alpha\beta}$, (2) for all remaining fields coupled to orbitals α or β swap the configurations $S_{\gamma\alpha} \leftrightarrow S_{\gamma\beta}$. Since the decoupling is anti-symmetric with respect to the ordering of orbitals, auxiliary fields must be flipped in step (2) whenever the order of orbitals changes between $S_{\gamma\alpha}$ and $S_{\gamma\beta}$.

Testing several types of the above moves we found that only simultaneous moves of two electrons between t_{2g} and e_g orbitals of opposite spin (i.e. moves intuitively expected in LS↔HS fluctuations) have appreciable acceptance. The acceptance rate of the global moves was found to be large only in the transition regime, which had been characterized by unusually slow convergence of the DMFT cycle. We checked for the possibility of multiple solutions, but found none at the temperature of these simulations. The numerical value of the total energy, limited by the stochastic error of the E_{DMFT} term, was converged to the accuracy of 0.06 eV in the transition regime and 0.02 eV anywhere else. The spectral densities were calculated by the maximum entropy analytic continuation technique[44] applied to the imaginary-time Green functions from $4 \times 10^7 - 6 \times 10^7$ QMC-simulation sweeps collected into 2000-20000 bins.

References

[*] Electronic address: jan.kunes@physik.uni-augsburg.de

[1] Mott N. F. The Basis of the Electron Theory of Metals, with Special Reference to the Transition Metals. Proc. Phys. Soc. (London) **A62**, 416 (1949).

[2] Mott N. F. Metal-insulator Transition. Rev. Mod. Phys. **40**, 677 (1968).

[3] Imada M., Fujimori A., and Tokura Y. Metal-Insulator Transitions. Rev. Mod. Phys. **70**, 1039 (1998).

[4] Saitoh T., Bouquet A. E., Mizokawa T., and Fujimori A. Systematic Variation of the Electronic Structure of 3d Transition-metal compounds. Phys. Rev. B **52**, 7934 (1995).

[5] Noguchi Y. Kusaba K., Fukuoka K., and Syono Y. Shock-induced Phase Transition of MnO around 90 GPa. Geophys. Res. Lett. **23**, 1469 (1996).

[6] Mita Y., Sakai Y., Izaki D., Kobayashi M., Endo S. and Mochizuki S. Optical Study of MnO Under Pressure. Phys. Stat. Sol. (B) **223**, 247 (2001).

[7] Mita Y. D. Izaki, M. Kobayashi, and S. Endo, Pressure-induced Metallization of MnO. Phys. Rev. B **71**, 100101 (2005).

[8] Patterson J. R., Aracne C. M., Jackson D. D., Malba V., Weir S. T., Baker P. A., and Vohra Y. K. Pressure-induced Metallization of the Mott Insulator MnO. Phys. Rev. B **69**, 220101 (2004).

[9] Yoo C. S., Maddox B. R., Klepeis J.-H. P., Iota V., Evans W., McMahan A., Hu M., Chow P., Somayazulu M., Häusermann D., Scalettar R. T., and Pickett W, E. First-order Isostructural Mott Transition in Highly Compressed MnO. Phys. Rev. Lett. **94**, 115502 (2005).

[10] Rueff J.-P., Mattila A., Badro J., Vankò G., and Shukla A. Electronic Properties of Transition-metal Oxides Under High Pressure Revealed by X-ray Emission Spectroscopy. J. Phys.: Cond. Matt. **17**, S717 (2005).

[11] Metzner W. and Vollhardt D. Correlated Lattice Fermions in $d = \infty$ Dimensions. Phys. Rev. Lett. **62**, 324-327 (1989).

[12] Georges A., Kotliar G., Krauth W., and Rozenberg M. J. Dynamical Mean-field Theory of Strongly Correlated Fermion Systems and the Limit of Infinite Dimensions. Rev. Mod. Phys. **68**, 13 (1996).

[13] Kotliar G. and Vollhardt D., Phys. Today **57**(3), 53 (2004).

[14] Lichtenstein A. I. and Katsnelson M. I. Ab initio Calculations of Quasiparticle Band Structure in Correlated Systems: LDA++ Approach. Phys. Rev. B **57**, 6884 (1998)

[15] Held K., McMahan A. K., and Scalettar R. T. Cerium Volume Collapse: Results from the Merger of Dynamical Mean-Field Theory and Local Density Approximation. Phys. Rev. Lett. **87**, 276404 (2001).

[16] Savrasov S. Kotliar G., and Abrahams E. Electronic Correlations in Metallic Plutonium within Dynamical

Mean-field Picture. Nature **410**, 793 (2001).

[17] Held K., Keller G., Eyert V., Vollhardt D., and Anisimov V. I. Mott-Hubbard Metal-Insulator Transition in Paramagnetic V2O3: An LDA+DMFT(QMC) Study. Phys. Rev. Lett. **86**, 5345 (2001).

[18] Georges A. Strongly Correlated Electron Materials: Dynamical Mean Field Theory and Electronic Structure. AIP Conference Proceedings **715**, 3-73 (2004).

[19] Held K., Nekrasov I. A., Keller G., Eyert V., Blumer N., McMahan A.K., Scalettar R. T., Pruschke Th., Anisimov V. I., and Vollhardt D. Realistic Investigations of Correlated Electron Systems with LDA+DMFT. Phys. Stat. Solidi b **243**, 2599 (2006).

[20] Kotliar G., Savrasov S. Y., Haule K., Oudovenko V. S., Parcollet O., and Marianetti C. A. Electronic Structure Calculations with Dynamical Mean Field Theory. Rev. Mod. Phys. **78**, 865 (2006).

[21] Kuneš J., Anisimov V. I., Lukoyanov A. V., and Vollhardt D., Local Correlations and Hole Doping in NiO: A Dynamical Mean Field Study. Phys. Rev. B **75**, 165115 (2007);

[22] Kuneš J., V. I. Anisimov, S. L. Skornyakov, A. V. Lukoyanov, and D. Vollhardt, NiO: Correlated Band Structure of a Charge-Transfer Insulator. Phys. Rev. Lett. **99**, 156404 (1997).

[23] Cohen R. E., Mazin I. I., and Isaak D. G., Magnetic Collapse in Transition Metal Oxides at High Pressure: Implications for the Earth. Science **275**, 654 (1997).

[24] Fang Z., Solovyev I. V., Sawada H., and Terakura K. First Principles Study on Electronic Structures and Phase Stability of MnO and FeO Under High Pressure. Phys. Rev. B **59**, 762 (1999).

[25] Kasinathan D., Kuneš J., Koepernik K., Diaconu C. V., Martin R. L., Prodan I. D., Scuseria G., Spaldin N., Petit L., Schulthess T. C., and Pickett W. E. Mott Transition of MnO under Pressure: Comparison of Correlated Band Theories. Phys. Rev. B **74**, 195110 (2006).

[26] Kasinathan D., Koepernik K., and Pickett W. E., Pressure-Driven Magnetic Moment Collapse in the Ground State of MnO. New J. Phys. **9**, 235 (2007).

[27] McMahan A. K., Held K., and Scalettar R. T. Thermodynamic and Spectral Properties of Compressed Ce Calculated Using a Combined Local-density Approximation and Dynamical Mean Field Theory. Phys. Rev. B **67**, 075108 (2003).

[28] McMahan A. K., Combined Local-density and Dynamical Mean Field Theory Calculations for the Compressed Lanthanides Ce, Pr, and Nd. Phys. Rev. B **72**, 115125 (2005).

[29] McMahan A. K., Held K., and Scalettar R. T. Thermodynamic and Spectral Properties of Compressed Ce Calculated using a Combined Local-density Approximation and Dynamical Mean-field Theory. Phys. Rev. B **67**, 075108 (2003).

[30] van Elp J., Potze R. H., Eskes H., Berger R., and Sawatzky G. A. Electronic Structure of MnO. Phys. Rev. B **44**, 1530 (1991).

[31] Liebsch A., Mott Transitions in Multiorbital Systems. Phys. Rev. Lett. **91**, 226401 (2003).

[32] Koga A., Kawakami N., Rice T. M., and Sigrist M. Orbital-Selective Mott Transitions in the Degenerate Hubbard Model. Phys. Rev. Lett. **92**, 216402 (2004).

[33] Anisimov V. I., Zaanen J., and Andersen O. K., Phys. Rev. B **44**, 943 (1991).

[34] Werner P. and Millis A. J. High-Spin to Low-Spin and Orbital Polarization Transitions in Multiorbital Mott Systems. Phys. Rev. Lett. **99**, 126405 (2007).

[35] Savrasov S. Y. and Kotliar G. Spectral Density Functionals for Electronic Structure Calculations. Phys. Rev. B **69**, 245101 (2004).

[36] Shick A., Havela L., Kolorenc J., Drchal V. Multiplet Effects in the Electronic Structure of δ-Pu, Am and their Compounds. Europhys. Lett. **77**, 5 (2007).

[37] Pavarini E., Biermann S., Poteryaev A., Lichtenstein A. I., Georges A., and Andersen O. K. Mott Transition and Suppression of Orbital Fluctuations in Orthorhombic $3d^1$ Perovskites. Phys. Rev. Lett. **92**, 176403 (2004).

[38] Craco L, Laad MS, Leoni S, Muller-Hartmann E. Insulator-metal Transition in the Doped $3d^1$ Transition Metal Oxide LaTiO-3. Phys. Rev. B **70**, 195116 (2004).

[39] Hirsch J. E. and Fye R. M. Monte Carlo Method for Magnetic Impurities in Metals. Phys. Rev. Lett. **56**, 2521 (1986).

[40] Anisimov V. I., Kondakov D. E., Kozhevnikov A. V., Nekrasov I. A., Z. V. Pchelkina V., Allen J. W., Mo S.-K., H.-D. Kim H.-D., Metcalf P., Suga S., Sekiyama A., Keller G., Leonov I., Ren, X., and Vollhardt D. Full Orbital Calculation Scheme for Materials with Strongly Correlated Electrons. Phys. Rev. B **71**, 125119 (2005).

[41] Shick A. B, Liechtenstein A. I. , and Pickett W. E. Implementation of the LDA+U Method Using the Full Potential Linearized Augmented Plane Wave Basis. Phys. Rev. B **60**, 10763 (1999).

[42] Anisimov V. I. and Gunnarsson O. Density Functional Calculation of Effective Coulomb Interactions in Metals. Phys. Rev. B **43**, 7570 (1991).

[43] Scalettar R. T., Noack R. M., and Singh R. R. Ergodicity at Large Couplings with the Determinant Monte Carlo Algorithm. Phys. Rev. B **44**, 10502 (1991).

[44] Jarrell M. and Gubernatis J. E. Bayesian Inference and the Analytic Continuation of Imaginary-Time Quantum Monte Carlo Data. Phys. Rep. **269**, 133 (1996).

Acknowledgments

J.K. gratefully acknowledges the Research Fellowship of the Alexander von Humboldt Foundation. We acknowledge numerous discussions with D. Vollhardt and A. K. McMahan, and useful interaction with K.-W. Lee during the latter stages of this work. This work was supported by SFB 484 of the Deutsche Forschungsgemeinschaft (J.K.), by the Russian Foundation for Basic Research under the grants RFFI-06-02-81017, RFFI-07-02-00041 (V.I.A. and A.V.L.) and the Dynasty Foun-

dation (A.V.L.), by DOE grant No. DE-FG02-04ER46111, and by DOE Strategic Science Academic Alliance grant No. DE-FG01-06NA26204. This research was also encouraged and supported by the U.S. Department of Energy's Computational Materials Science Network (J.K., R.T.S., and W.E.P.).

Competing financial interests

The authors declare no competing financial interests.

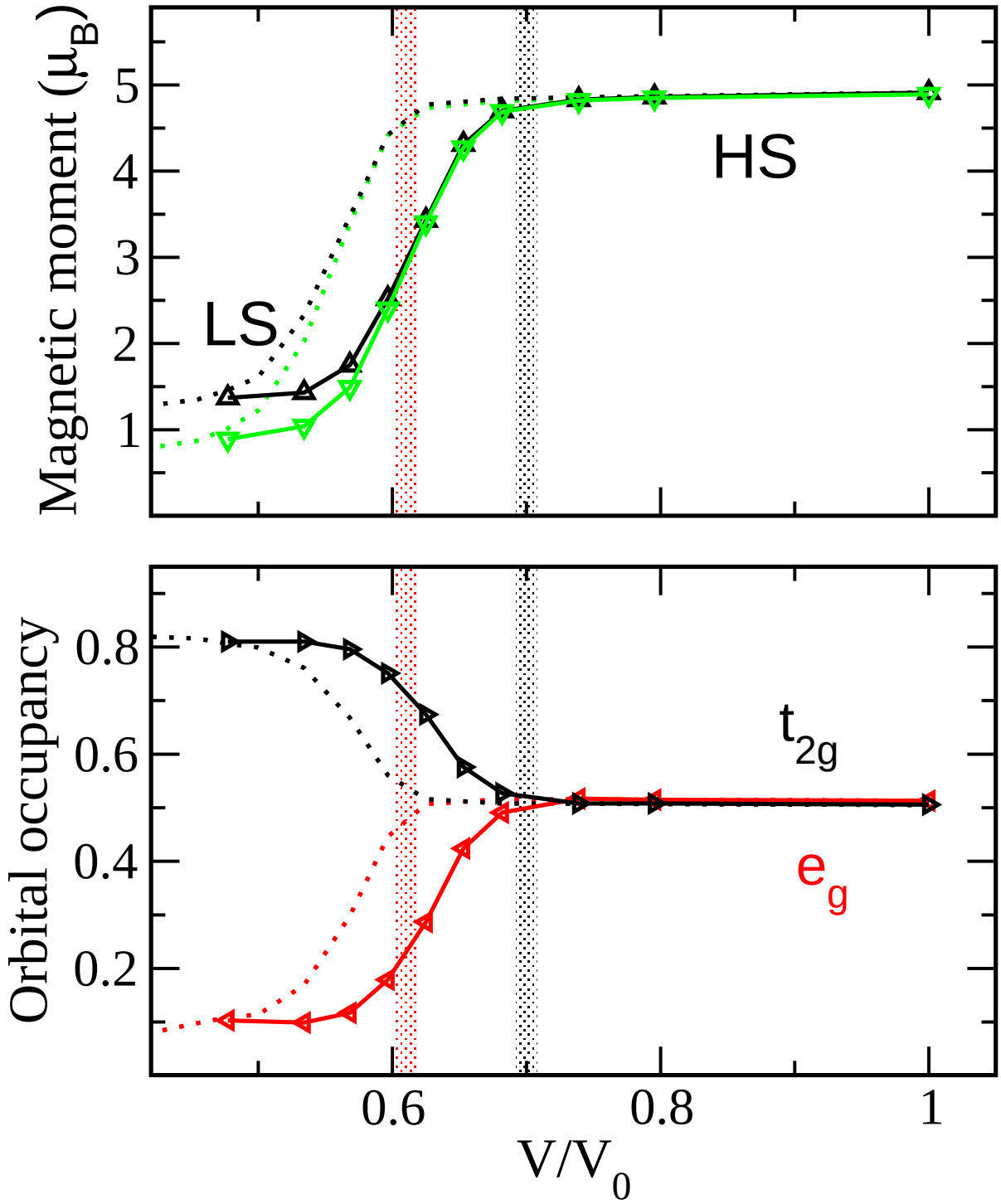

FIG. 1: This figure shows how the decrease in the local moment correlates with the orbital occupations, which reveal the spin state with relative volume.. The upper panel gives average instantaneous local moment M_s (black) and effective local moment M_{eff} (green), and comparison to the Mn $3d$ orbital occupancies (lower panel) resolved into e_g (red) and t_2g (black) components. The solid lines represent the results obtained with the physical values U=6.9 eV, J=0.86 eV; the dashed lines using the enhanced value J=1 eV and constant U/J ratio illustrates how the moment collapse is suppressed to smaller volume if the spin-exchange coupling is increased. Closing of the t_{2g} and e_g gaps is indicated by the black and red vertical lines respectively, confirming a connection between metallization and moment collapse. The analogous closing of the gaps for the dotted line case (J=1 eV) is shifted correspondingly (not shown here).

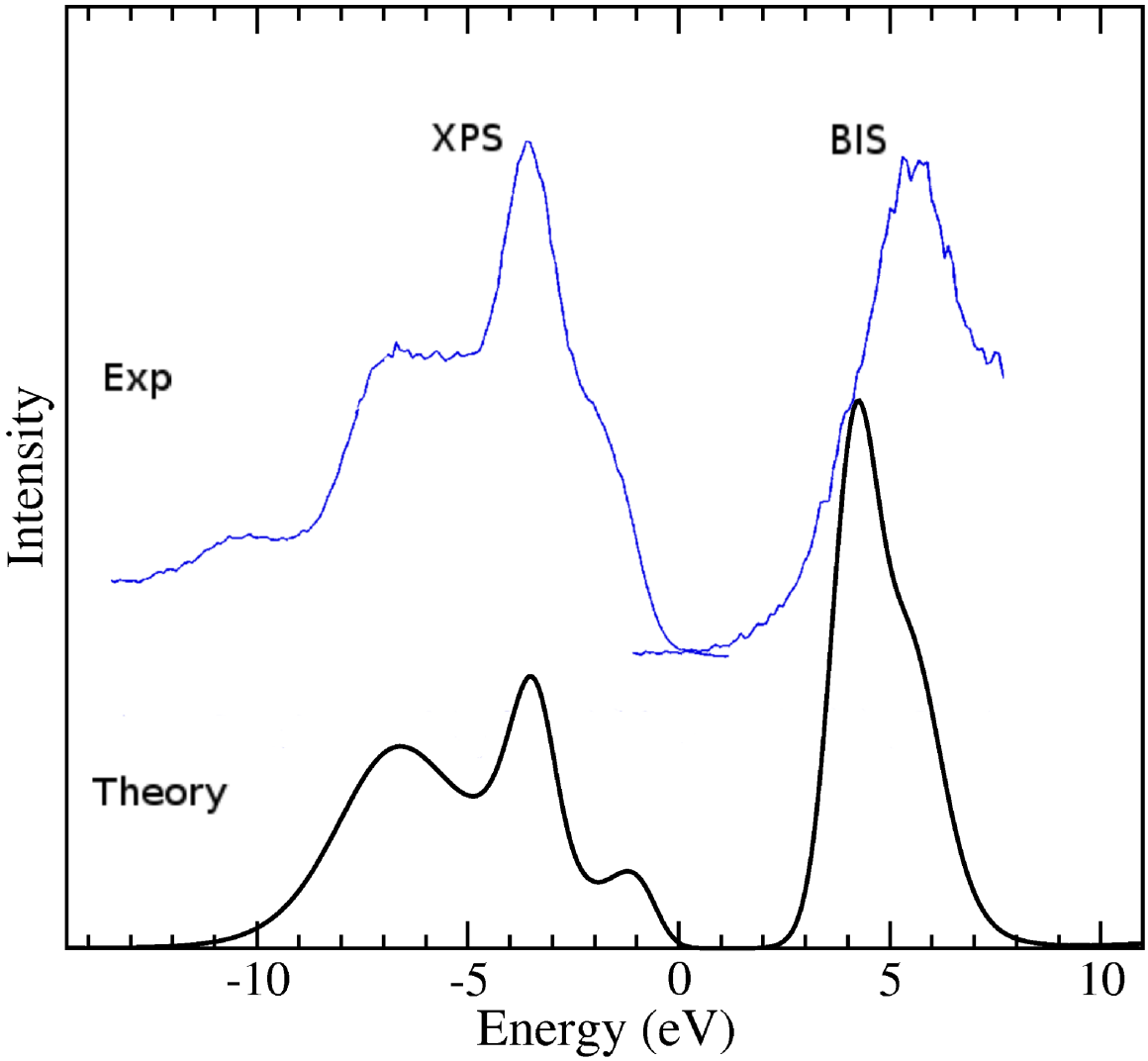

FIG. 2: Ambient pressure x-ray photoemission spectroscopy (XPS) and bremsstrahlung isochromat spectroscopy (BIS) data of van Elp *et al.*[30] on both sides of the energy gap for MnO. The upper curve, offset for clarity, is to be compared with the present DMFT result (bottom curve). While the separation of the main peaks is underestimated by $\sim 10\%$, the overall agreement in positions of structure is excellent.

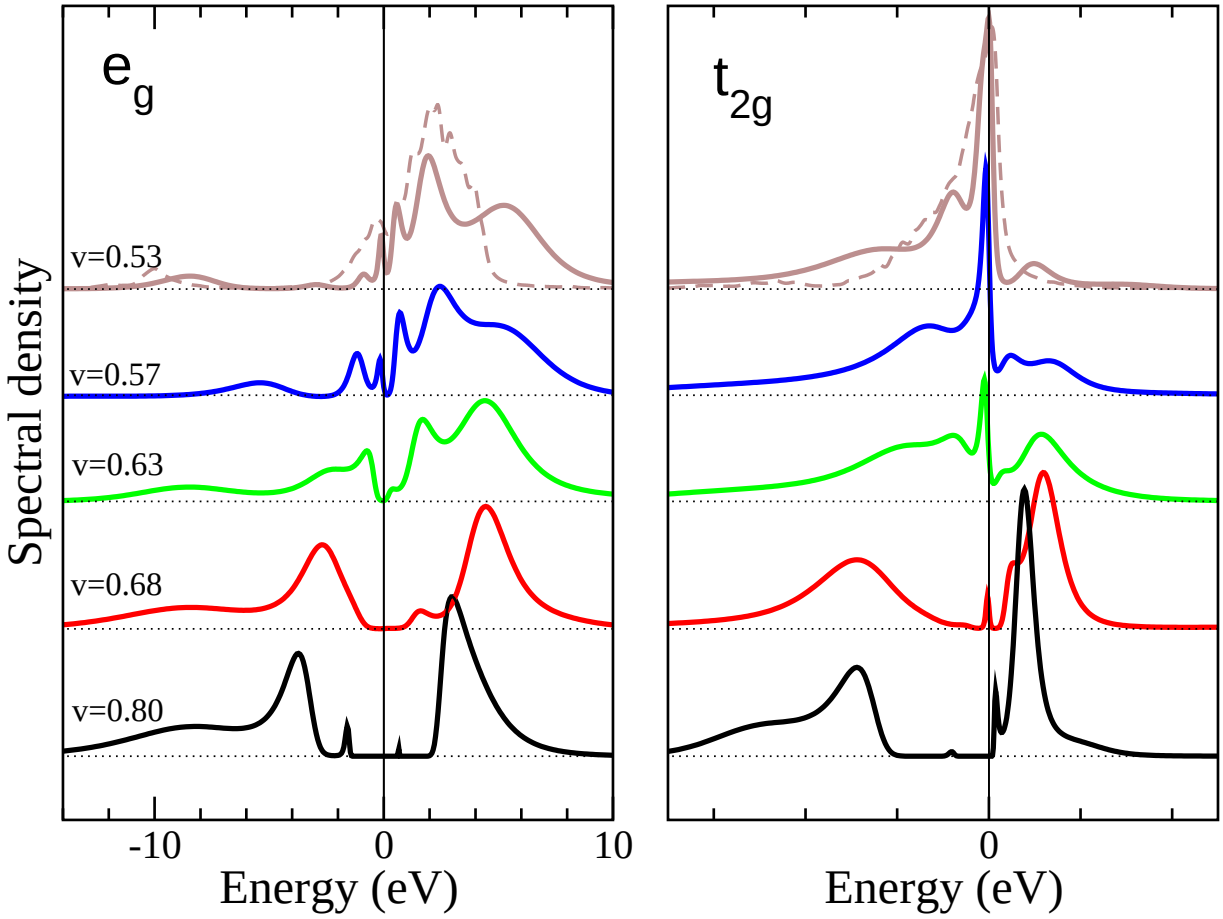

FIG. 3: View of the evolution of the Mn $3d$ spectral densities under pressure (pressure increasing from bottom to top). The single-particle spectral functions are resolved into e_g (left) and t_{2g} (right) irreducible representations for varying relative volume. Note the spectral weight shift under pressure: de-occupation of e_g occurs as the increase in occupation of t_{2g} proceeds (occupation $\equiv$ integrated weight over negative energies). For the lowest volume we show the uncorrelated (LDA) spectra for comparison (dotted lines). Apparently the main spectral features at high pressure originate from the uncorrelated band structure with some many-body renormalization. At even higher pressures the spectra remain qualitatively unchanged with some reduction of the weight of the high energy shoulders.

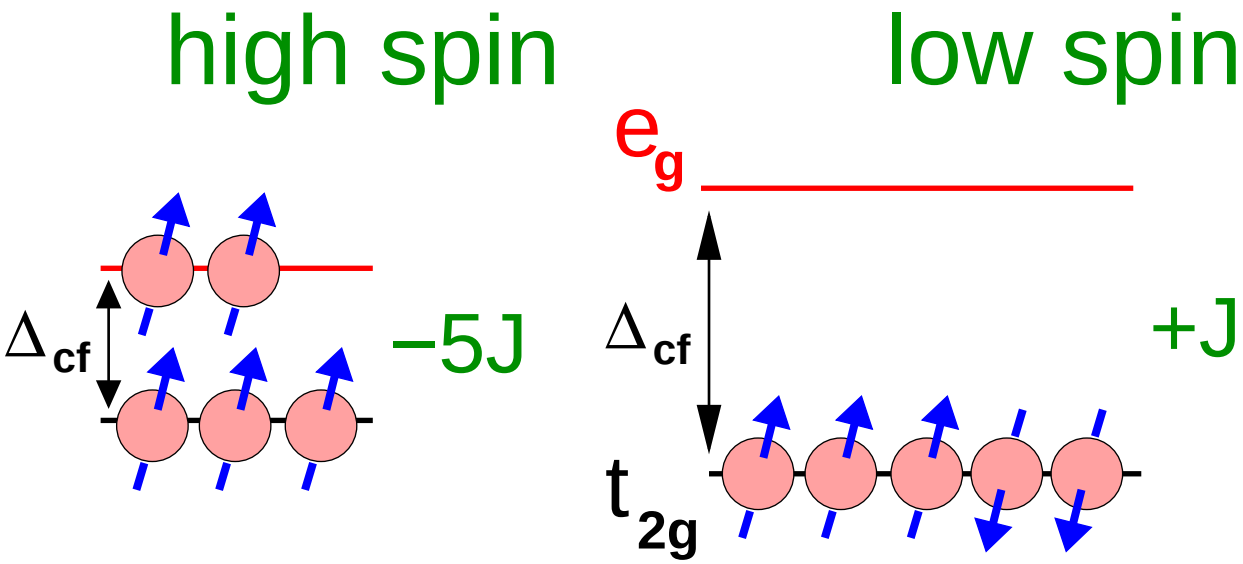

FIG. 4: Schematic energy diagrams of the spin states at both ambient pressure and at high pressure in the collapsed phase. Occupations of the Mn $3d$ levels are pictured for both high spin (left) and low spin (right). In the HS state two spin-up electrons occupy e_g orbitals at the cost of $2\Delta_{cf}$ in energy, but the spin-exchange energy gain is -10J (5×4/2 = 10 pairs of parallel spin electrons). In the LS state, the crystal field energy cost has become too great, and although the spin-exchange energy is less [-4J from 3×2/2 (up) + 1 (down) = 4 pairs] there is a net energy gain. The LDA energy difference is also a factor.

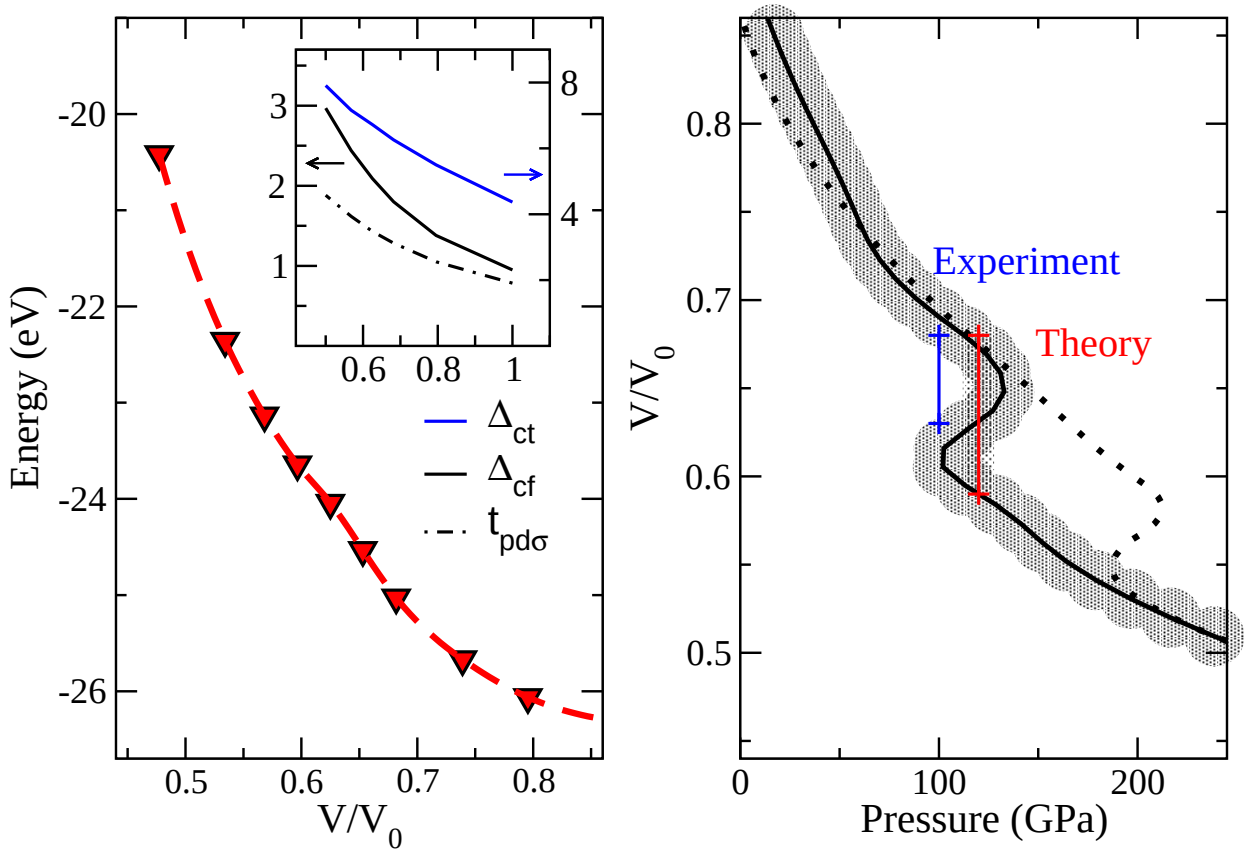

FIG. 5: The equation of state that quantifies the volume collapse transition is presented in two representations. In the left panel is the internal energy versus volume (dashed line represents a spline interpolation), and the right panel shows the resulting volume versus pressure curve (shading indicates estimated uncertainty), obtained as a derivative of the spline interpolation of E(V). The red bar on the $V(P)$ curve lying at the theoretical transition pressure $P_c^{th} = 120 \pm 15$ GPa determines the volume collapse $v = 0.68 \rightarrow 0.59$. The dotted curve represents $V(P)$ for the enhanced value of exchange J=1 eV, showing the shift of the Mott transition to higher pressure with larger J. Width of the shaded red bar indicates the uncertainty of P_c^{th} due to stochastic nature of QMC. The inset in the left panel shows the evolution of selected tight-binding parameters (units of eV); note specifically the factor of three increase in Δ_{cf} .